Reproducible Coactivation Patterns of Functional Brain Networks Reveal the Aberrant Dynamic State Transition in Schizophrenia

Hang Yang[1], Hong Zhang[1], Xin Di[1,2], Shuai Wang[3], Chun Meng[1*], Lin Tian[3*], Bharat Biswal[1,2*]

[1] The Clinical Hospital of Chengdu Brain Science Institute, MOE Key Laboratory for Neuroinformation, Center for Information in Medicine, School of Life Science and Technology, University of Electronic Science and Technology of China, Chengdu 611731, China.

[2] Department of Biomedical Engineering, New Jersey Institute of Technology, Newark, NJ, 07102, USA.

[3] Department of Psychiatry, The Affiliated Wuxi Mental Health Center of Nanjing Medical University, Wuxi 214151, China

* **Correspondence:**

Dr. Chun Meng, The Clinical Hospital of Chengdu Brain Science Institute, MOE Key Laboratory for Neuroinformation, Center for Information in Medicine, School of Life Science and Technology, University of Electronic Science and Technology of China, No. 2006, Xiyuan Avenue, Chengdu 611731, China; E-mail: chunmeng@uestc.edu.cn

Dr. Lin Tian, Department of Psychiatry, The Affiliated Wuxi Mental Health Center of Nanjing Medical University, No. 156 Qianhu Road, Binhu District, Wuxi 214151, China; E-mail: tianz@njmu.edu.cn

Dr. Bharat B. Biswal, 607 Fenster Hall, University Height, Newark, NJ, 07102, USA; E-mail: bbiswal@yahoo.com

Highlights:

1. Three coactivation patterns (CAPs) pairs with opposite coactivation profiles were identified, and the between-state transition probability was positively correlated with their spatial similarity.

2. Good spatial and temporal reproducibility and generalizability of CAPs were achieved under varied analytic methods and independent cohorts.

3. Schizophrenia patients showed altered temporal dynamics not only within the triple-network but also other primary and higher-order networks.

Abstract

It is well documented that massive dynamic information is contained in the resting-state fMRI. Recent studies have identified recurring states dominated by similar coactivation patterns (CAP) and revealed their temporal dynamics. However, the reproducibility and generalizability of the CAP analysis is unclear. To address this question, the effects of methodological pipelines on CAP are comprehensively evaluated in this study, including preprocessing, network construction, cluster number and three independent cohorts. The CAP state dynamics are characterized by fraction of time, persistence, counts, and transition probability. Results demonstrate six reliable CAP states and their dynamic characteristics are also reproducible. The state transition probability is found to be positively associated with the spatial similarity. Furthermore, the aberrant CAP in schizophrenia has been investigated by using the reproducible method on three cohorts. Schizophrenia patients spend less time in CAP states that involve the fronto-parietal network, but more time in CAP states that involve the default mode and salience network. The aberrant dynamic characteristics of CAP are correlated with the symptom severity. These results reveal the reproducibility and generalizability of the CAP analysis, which can provide novel insights into the neuropathological mechanism associated with aberrant brain network dynamics of schizophrenia.

Keywords: coactivation patterns, dynamics, reproducibility, schizophrenia, triple-network

1. Introduction

Since the resting-state fMRI was confirmed to be physiologically meaningful,(B. Biswal et al., 1995) a number of resting-state fMRI studies have emerged, of which functional connectivity (FC) is one popular method to detect the remote functional co-fluctuations (B. B. Biswal et al., 2010; Friston, 2011). Previous functional connectivity methods have typically assumed stationarity that the time series do not change their characteristics over time. However, the brain is indeed a complex system featured by the dynamic functional brain connectome (Zalesky et al., 2014). Recent evidence suggests that functional interactions between different brain regions and networks vary with time. The sliding-window based dynamic functional connectivity (dFC) is intensively used to measure the dynamic interaction between two regions (Hutchison et al., 2013; Preti et al., 2017), which has been shown to link with individual differences (Fong et al., 2019), task performances and disease alterations (Gonzalez-Castillo & Bandettini, 2018).

Despite the limitation of the sliding-window approach, the dynamic characteristics of the functional brain connectome at the macroscopic level support that the brain has multiple functional recurring states (Zalesky et al., 2014). There are several methods for dynamic brain state detection. Combining the sliding-window dFC with the clustering method, Allen and colleagues identified several FC states, as an intermediate scale between static and instant FC underlying small short-time tasks, which can reallocate and integrate attentional and executive resources (Allen et al., 2014). Besides, based on the assumption of temporal independence, Smith and colleagues used temporal ICA to identify temporal function modes (TFM), which represent unique brain activation patterns (Smith et al., 2012). Different from the dFC-clustering and TFM which assign each time point to one single state, the approach of the hidden Markov model (HMM) could identify a mixture of the brain states with a given probability at each time point, by assuming the transitions between states should follow a Markov process (Vidaurre et al., 2016). Vidaurre et al. used HMM in resting-state fMRI, and they found two hierarchical metastates that represent higher-order cognition and sensorimotor systems (Vidaurre et al., 2017).

The coactivation pattern (CAP) analysis is a data-driven method to detect the functional brain states in a single volume level (Liu et al., 2013; Liu & Duyn, 2013), which originates from the point process analysis (Tagliazucchi et al., 2012). Rather than capturing the dFC configurations as brain states, it is simple and straightforward that, for each frame of the data, the spatial coactivation patterns represent a specific whole-brain activation configuration to deal with the real-time task at that time, and that different frames which share the same spatial

3

91   patterns are regarded as the same CAP state (Figure 1A). As a data-driven method, CAP

92   analysis relies on very few mathematical presumptions, and is free of the confounding

93   influence from the sliding window length. Therefore, CAP analysis has increasingly been

94   used to study the abnormal network dynamics in depression (Kaiser et al., 2019), Alzheimer's

95   disease (Kaiser et al., 2019; Ma et al., 2020) and task fMRI (Freitas et al., 2020).

96   The reproducibility is crucial for analytical methods in fMRI studies (Botvinik-Nezer et

97   al., 2020; Eklund et al., 2016; Zuo et al., 2019). A lot of analytic flexibility exists in fMRI

98   studies (Vergara et al., 2017), such as different preprocessing pipelines (Shirer et al., 2015),

99   different software and toolboxes (Bowring et al., 2019). It is necessary to clarify the effects of

100   varied settings in neuroimaging analyses (Aurich et al., 2015; Strother, 2006; Vergara et al.,

101   2017) and to establish a standard and robust methodological pipeline (Esteban et al., 2019).

102   However, it still remains unknown about the analytic flexibility and reproducibility for CAP

103   analysis.

104   Schizophrenia is a psychiatric disorder with complex structural and functional brain

105   alterations, characterized by abnormal connectome and functional dynamics (Collin et al.,

106   2016; Fornito et al., 2012; Hunt et al., 2017). Particularly, the triple-network (V. Menon,

107   2011), including the default-mode network (DMN), fronto-parietal network central (FPN) or

108   executive network (CEN), and salience network (SN), is postulated as a critical core of

109   network dysfunction for understanding the neuropathological mechanism of psychiatric

110   disorders including schizophrenia (Manoliu et al., 2014; V. Menon, 2011). Recently, Supekar

111   and colleagues found that reduced dynamic interactions among the SN, CEN and DMN may

112   substrate neurobiological signatures of schizophrenia (Supekar et al., 2019). However, little is

113   known about the aberrant dynamic characteristics in schizophrenia concerning triple networks

114   as well as other parts of the whole brain.

115   This study aimed to first investigate the reproducibility and generalizability of the CAP,

116   and then utilize the robust analytical approach to study the aberrant dynamic state transition in

117   schizophrenia. To achieve this goal, key methodological aspects were carefully evaluated for

118   the robustness of CAP, including different preprocessing pipelines, ROI numbers for network

119   construction, cluster numbers, and cohorts. Then, reliable dynamic states in the functional

120   brain coactivation patterns were identified and further employed to compare the temporal

121   dynamic characteristics between schizophrenia patients (SZ) and healthy controls (HC) in

122   three independent data cohorts. Next, the associations between aberrant dynamic state

123   transition and clinical symptom severity were explored.

124

4

2. Materials and Methods

2.1 Participants

To explore the reproducibility and generalizability of this study, three cohorts (WuXi, COBRE and UCLA) were analyzed. The WuXi cohort was used as the primary cohort, the other two open-access cohorts were treated as verification and their detailed participant information was described in the Supplementary material.

For the primary cohort (WuXi), all subjects were scanned by a structural MRI and resting-state functional MRI on a 3.0-Tesla Magnetom TIM Trio (Siemens Medical System) at the Department of Medical Imaging, Wuxi People's Hospital, Nanjing Medical University. Foam pads were used to reduce head motion and scanner noise. Before the scan, the subjects were instructed to keep their eyes closed, relax but not fall asleep, and move as little as possible during data acquisition. After excluding subjects with large head motion, 69 SZ subjects and 97 HC subjects remained for the current study. Positive and Negative Syndrome Scale (PANSS) was used to measure the psychiatric symptoms of SZ patients.

Framewise displacement (FD) was calculated from the resting-state fMRI data to measure head motion (Di & Biswal, 2015). Subjects were excluded if their maximum translation or rotation FD were greater than 2 mm or 2°. The k-means clustering was performed in all 97 HC subjects. For the group comparisons between SZ and HC, only age- and gender-matched HC subjects were analyzed. The age- and gender-matched demographic information for the three cohorts were provided in Table 1. The information for all HC subjects used in the coactivation patterns generation can be found in the Supplementary material.

2.2 fMRI Data Acquisition

for the primary cohort (WuXi), the resting-state scans were acquired using a single-shot gradient-echo echo-planar-imaging sequence (Tian et al., 2016) with the following parameters: TR = 2000 ms, TE = 30 ms, slice number = 33, slice thickness = 4 mm, flip angle = 90°, matrix size = 64 × 64, FOV = 220 mm, voxel size = $3.4 \times 3.4 \times 4$ mm^3, and volume number = 240. Three-dimensional T1-weighted images were acquired by employing a 3D-MPRAGE sequence with the following parameters: TR = 2530 ms, TE = 3.44 ms, flip angle = 7°, matrix size = 256 × 256, slice number = 192, slice thickness = 1 mm, FOV = 256 mm, and voxel size = $1 \times 1 \times 1$ mm^3. The fMRI data acquisition parameters for the other two cohorts were described in the Supplementary material.

2.3 fMRI Data Preprocessing

The resting-state fMRI data were preprocessed using DPABI (http://rfmri.org/dpabi), and the preprocessing steps were followed: 1) Remove the first 2 time points for the UCLA and COBRE dataset, and remove the first 5 time points for the WuXi cohort; 2) Realignment; 3) Coregisteration of T1 image to functional image; 4) T1 segmentation by DARTEL; 5) Normalization of the functional images by T1 DARTEL; 6) Nuisance regression, including 24 head motion parameters, mean white matter (WM) and mean cerebrospinal fluid (CSF) signal, both with and without global signal regression (GSR); 7) Detrend; 8) Band-pass filtering, from $0.01 \sim 0.08$ Hz; 9) Smoothing with an 8 mm FWHM kernel.

To evaluate the effect of preprocessing steps, the resting-state fMRI data was also preprocessed using a standard task fMRI data preprocessing pipeline, which is similar to the above steps but without nuisance regression and filtering.

The BOLD signal for the preprocessed resting-state fMRI data was extracted from 408 ROIs separately. The 408 ROIs were consist of 400 cortical regions from Yeo's 7 network parcellation (Schaefer et al., 2018) and 8 subcortical regions (bilateral caudate nucleus, putamen, globus pallidus and amygdala) from the AAL template (Tzourio-Mazoyer et al., 2002). The 400 cortical regions are allocated to 7 networks including the visual network (VN), somatomotor network (SMN), dorsal attention network (DAN), ventral attention network (VAN), limbic network, fronto-parietal network (FPN) and default mode network (DMN) (Yeo et al., 2011). The 7 networks have parcellations with different spatial scales from 100 to 1000, and 400 was mainly used in this study because the average voxel size for the 400 ROIs is comparable to the average voxel size of the 8 subcortical regions from the AAL template.

2.4 Coactivation Pattern Analysis

Coactivation pattern (CAP) analysis is a data-driven method that identifies recurring states across time points with similar whole-brain coactivation patterns. In this study, the CAP analysis was performed using home-made scripts in MATLAB (https://www.mathworks.com/).

First, to represent the relative activation magnitude changes in the 408 ROIs, each time series were normalized using a z-score. For each subject i, a two-dimensional normalized BOLD matrix X_i ($T \times 408$) was obtained, where T is the number of time points and 408 is the ROI number.

192   Next, all HC subjects' normalized BOLD metrics X_{HC_i} ($T \times 408$) were concatenated to

193   obtain the X_{HC} ($T_{HC} \times 408$, $T_{HC} = T \times N$), where N is the sample size of all HC subjects. Then,

194   k-means clustering was performed to identify similar coactivation patterns across all volumes

195   from all HC subjects, and the distance between two volumes was calculated by subtracting

196   their Pearson correlation coefficient from one. The cluster number K was selected from 2 to

197   21 with a step length of 1. The clustering algorithm was repeated 100 times with a new initial

198   cluster centroid for each K value, and the results with the lowest within-cluster sums of point-

199   to-centroid distances were used. Frames assigned to the same CAP state were averaged and

200   divided by the within-cluster standard deviation to generate the normalized CAP maps (Z-

201   maps) at the group level (Figure 1A).

202   The clustering patterns obtained from all HC subjects were then applied to each SZ

203   subject. Specifically, each frame from the X_{SZ_i} ($T \times 408$) was extracted, which is a 1×408

204   vector representing the whole-brain coactivation level at that time point. Then, the spatial

205   similarity between each frame and each normalized CAP map was calculated using the

206   Pearson correlation, and the frame was assigned to the CAP with the largest spatial similarity.

207   The silhouette score (Rousseeuw, 1987) was calculated to evaluate the clustering results

208   for different K values. As shown in Figure S1, Supplementary material, the silhouette score

209   was monotonically decreasing with the increase of K. Then, the elbow criterion was

210   considered to determine the number of clusters. While one issue is that the time points of the

211   three cohorts are limited, if the cluster number is too large, then each CAP state would only

212   account for a few seconds through the entire scan. Therefore, 6 clusters were mainly analyzed

213   and reported in the manuscript as a trade-off, and one recent paper also used 6 clusters for the

214   CAP analysis (Zhang et al., 2020).

215

216   **2.5 State Temporal Dynamics Measures / CAP Metrics:**

217   To evaluate the dynamic properties within and between CAP states, four dynamic

218   measures (CAP metrics) were calculated at the individual level: 1) **Fraction of time** is

219   defined as the proportion of total volumes spent in one CAP state over the whole time series;

220   2) **Persistence** is the average time spent in one state before transferring to another state, and it

221   describes the mean volume-to-volume maintenance of one CAP state; 3) **Number of states**

222   **(Counts)** is how many times one state occurred during the whole scan; and 4) **Transition**

223   **probability matrix** is the probability that one volume within State A transfers to the next

224   volume belonging to State B, with a non-zero diagonal as the volume within State A could

225   still stay within State A for the next volume.

226

2.6 Transition Probability and Spatial Similarity between States

The relationship between the spatial similarity and transition probability between two states was measured in all HC subjects. The spatial similarity between different brain states was calculated using the Pearson correlation. Before measuring the relationship between the two metrics, the symmetry of the transition probability was first examined. In detail, the transition probability from State A to State B was paired with the transition probability from State B to State A, and the Pearson correlation was calculated between all pairs to test the symmetry level. The transition probability metrics were then averaged on the group level and symmetrized. Finally, the relationship between the spatial similarity and transition probability was measured using the Pearson correlation. The diagonal values were not analyzed in this part.

2.7 Reproducibility Analysis

Recently, neuroimaging studies have drawn more attention to reproducibility. In this study, the CAPs' spatial and temporal reproducibility were considered from four aspects. The first aspect is to consider the effects of different data preprocessing steps, including two standard resting-state fMRI preprocessing pipelines (with and without GSR) and one classic task fMRI preprocessing pipeline. Then, the effects of different spatial resolutions of the template were assessed. In detail, 100, 200, 400 and 1000 ROIs from Yeo's 7 network parcellations (Schaefer et al., 2018) plus the 8 subcortical regions from the AAL atlas (Tzourio-Mazoyer et al., 2002) were tested. Different K values were also compared to see whether the CAP states gradually change with the increase of cluster number. Finally, the CAP analysis was performed in three independent cohorts separately to detect the site effect.

Furthermore, to verify the generalizability of this study, whether the results obtained by one cohort can be directly replicated in other cohorts, we applied the CAPs generated from the WuXi cohort to the other two cohorts, then the spatial maps and temporal dynamics among CAP states were compared.

The spatial reproducibility was assessed by calculating the Pearson correlations between CAPs' spatial maps under different conditions, and the temporal dynamics were then compared between spatial matched CAPs.

2.8 Statistical Analysis

8

259   For group comparisons, only age- and gender-matched HC and SZ subjects were

260   analyzed. Age was compared between SZ and HC by a two-sample t-test, and a chi-square

261   cross-table test was used to test the gender difference. As for the CAP metrics, two-sample t-

262   tests were performed with age and gender as covariates. FDR correction (q = 0.05) was used

263   to correct for the multiple comparisons.

264   The relationship between CAP metrics and behavioral measures, such as disease

265   symptoms and disease duration, were tested using partial correlation with age and gender as

266   covariates. The state temporal dynamics and behavioral measures were first normalized using

267   z-score, and subjects with large deviation (Z > 3) were excluded in the correlation analysis as

268   the outlier. FDR correction (q = 0.05) was used to correct for the multiple comparisons.

269

3. Results

3.1. Demographics and Questionnaires

272   No group differences of age or gender were found between the SZ and HC in all three

273   cohorts, and the detailed group characteristics are given in Table 1.

274

275   **Table 1.** The demographic information for the three cohorts

	HC	SZ	P value
WuXi cohort (*n* = 138)			
Num of subjects	69	69	
Age [years]	45.84 ± 11.89	46.06 ± 10.96	0.9112[a]
Gender (Male / Female)	35 / 34	35 / 34	1[b]
Disease duration	-	19.84 ± 10.96	-
PANSS positive	-	20.06 ± 4.59	-
PANSS negative	-	23.78 ± 3.84	-
PNASS general	-	41.67 ± 5.27	-
PNASS total	-	85.51 ± 9.50	-
COBRE cohort (*n* = 108)			
Num of subjects	54	54	
Age [years]	37.22 ± 12.48	37.80 ± 14.13	0.8234[a]
Gender (Male / Female)	43 / 11	43 / 11	1[b]
Disease duration	-	15.19 ± 12.46	-
PANSS positive	-	14.13 ± 4.29	-
PANSS negative	-	14.46 ± 5.10	-
PNASS general	-	28.57 ± 8.40	-
PNASS total	-	57.17 ± 13.52	-
UCLA cohort (*n* = 90)			
Num of subjects	45	45	
Age [years]	36.73 ± 8.65	37.00 ± 8.75	0.8973[a]
Gender (Male / Female)	33 / 12	33 / 12	1[b]
BPRS	-	50.40 ± 14.08	-
SAPS	-	28.89 ± 18.49	-
SANS	-	35.09 ± 18.55	-

276   Data are expressed as mean ± SD (SD: standard deviation).

Abbreviations: BPRS, Brief Psychiatric Rating Scale; SANS, Scale for the Assessment of Negative Symptoms; SAPS, Scale for the Assessment of Positive Symptoms; PANSS, Positive and Negative Syndrome Scale.

[a)] two-sample t-test; [b)] chi-square cross-table test.

3.2. Reliable CAP identification and Dynamic Characteristics

This study tested different methodological combinations on three independent data cohorts, such as preprocessing pipelines, ROI numbers and cluster numbers. Below we reported the primary results of six reliable CAP states, which are based on the WuXi cohort, using the resting-state preprocessing with global signal regression (GSR) and 408 ROIs. The other validation results are provided in the Supplementary material.

3.2.1. Coactivation Patterns and Brain States

The coactivation patterns were generated from all HC subjects using temporal k-means clustering, and six CAP states were finally identified (Figure 1B), after the search for optimal cluster number (see details in the Supplementary material). Among the six CAP states, brain regions that belong to the same functional network, such as the default mode network (DMN), fronto-parietal network (FPN), and salience network (SN), tend to be activated or deactivated simultaneously. One interesting phenomenon is that the six CAP states were grouped into three pairs with opposite spatial coactivation patterns. For example, State 1 and 2 grouped together - State 2 was mainly related with the activated FPN, DMN (without posterior cingulate cortex and precuneus) and deactivated visual network (VN), while State 1 had the opposite spatial pattern. Since each CAP state had certain brain networks with relatively stronger activation or deactivation than the other networks of the whole brain, we found that not only triple networks but also primary (VN, SMN) and higher-order networks (DAN) were identified in the dominant CAP states.
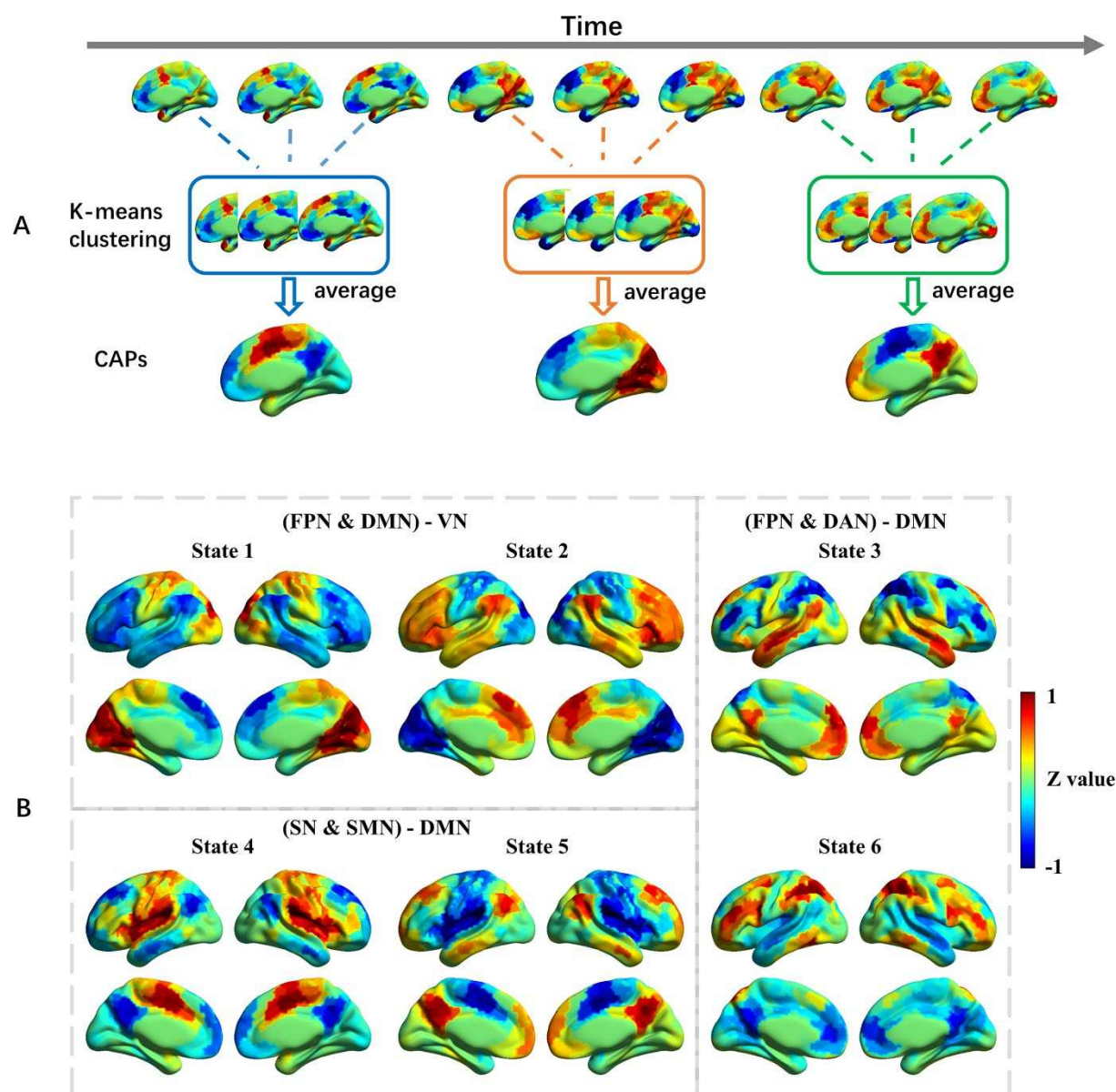
Figure 1 A) An illustration for the CAP analysis. The normalized spatial map for each volume was input for the k-means clustering, to identify volumes with similar coactivation patterns, and then average them to generate the CAPs. B) Six CAP states were identified by CAP analysis based on the primary configuration (WuXi cohort, resting-state fMRI preprocessing with GSR and 408 ROIs for the network construction). These brain states were normalized at the group level, and the value is the z-statistic value. Red color indicates a relatively stronger activation, while blue color indicates a relatively stronger deactivation. State 1 was mainly related to deactivated FPN, DMN and activated VN, and the opposite is true for State 2; State 3 was mainly characterized by activated DMN and deactivated FPN and DAN, and the opposite is true for State 6; State 4 was mainly characterized by deactivated DMN and activated SN and SMN, and the opposite is true for State 5.

316   Abbreviations: DAN, dorsal attention network; DMN, default mode network; FPN, fronto-

317   parietal network; SN, salience network; SMN, somatomotor network; VN, visual network.

318

319   *3.2.2. Transition Probability and Spatial Similarity between States*

320   As shown in the diagonal of the transition probability matrix (Figure 2A), the temporal

321   activity was dominated by the identified CAP states (more than 60% of the time), and the

322   between-state alteration remained low transition probability (1% to 11 % of the time).

323   Comparing Figure 2A and Figure 2B, it is clear that the transition probability between brain

324   states with strong anti-correlated spatial coactivation was close to zero. Taking State 4 and

325   State 5 for an example (Figure 2C), their coactivation patterns were opposite (spatial

326   similarity r = - 0.99), their transition probability from State 4 to State 5 was 0.0081, and from

327   State 5 to State 4 was 0.0103. Despite the small discrepancy in bi-directional transition

328   probability, the symmetry in the transition probability matrix is pronounced. Figure 2D

329   showed a significant positive correlation (r = 0.8479, p < 0.0001) between the transition

330   probability from State A to State B and transition probability from State B to State A. Finally,

331   the relationship between the transition probability and spatial similarity metrics was

332   evaluated. As shown in Figure 2E, the transition probability between two CAP states was

333   highly correlated with their spatial similarity (r = 0.9817, p < 0.0001).
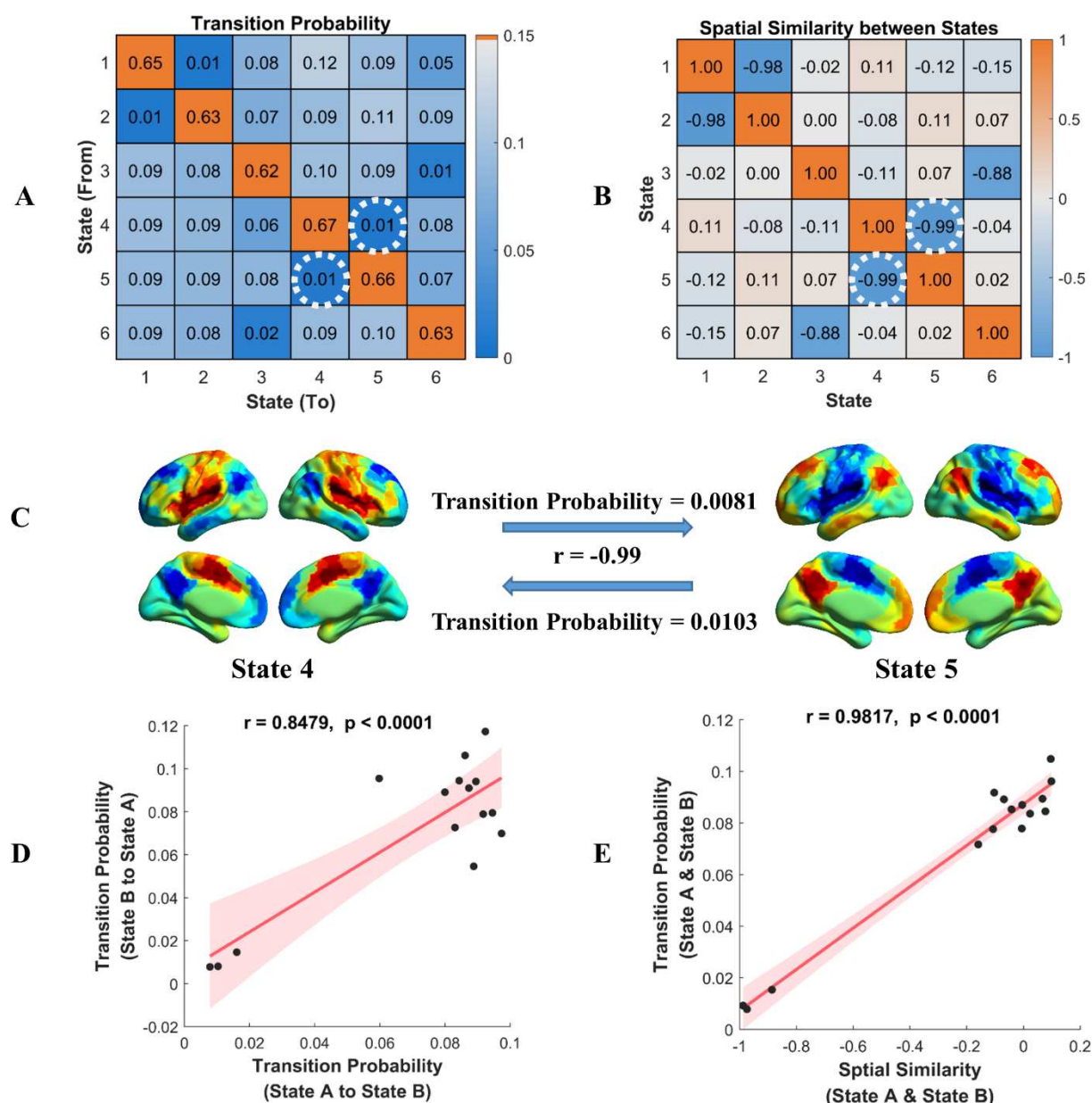
334

Figure 2. The relationship between CAP state transition probability and their spatial similarity. A) The group average transition probability matrix in all HC subjects. B) The spatial similarity between six CAP states, measured by the Pearson correlation. C) The transition probability between State 4 and State 5, and their spatial similarity, the values were shown in the white dashed circles in Figure 2A and Figure 2B. D) The correlation between transition probability from State A to State B and transition probability from State B to State A. The shadow represents the 95% confidence interval. E) The correlation between the symmetrized transition probability between State A and State B and their spatial similarity. The shadow represents the 95% confidence interval.

3.2.3. Spatial Reproducibility Evaluation

13

347   As shown in Figure 3, each row or column showed two pairs with high spatial similarity,

348   which suggest reproducible CAP states and their groups. It indicated that good spatial

349   reproducibility within the HC group remained across different preprocessing pipelines and

350   ROI numbers for network construction.

351   Moreover, the validation analysis for different cluster number K also demonstrated good

352   spatial reproducibility, although more CAP states were separated with the increase of K. For

353   example, as shown in Figure 6, when K increased from 6 to 8, four states (State 3 to State 6)

354   remained unchanged, their one-to-one correspondence spatial similarity was larger than 0.9,

355   and the other two states (State 1 and State 2) were subdivided into four states.

356   To evaluate the reproducibility and generalizability of identified CAP states, the

357   clustering results from the WuXi cohort were applied to all subjects from the COBRE cohort

358   and UCLA cohort. The diagonal of metrics in Figure 7A showed the high spatial similarity of

359   each CAP state between the WuXi cohort and the other two cohorts.
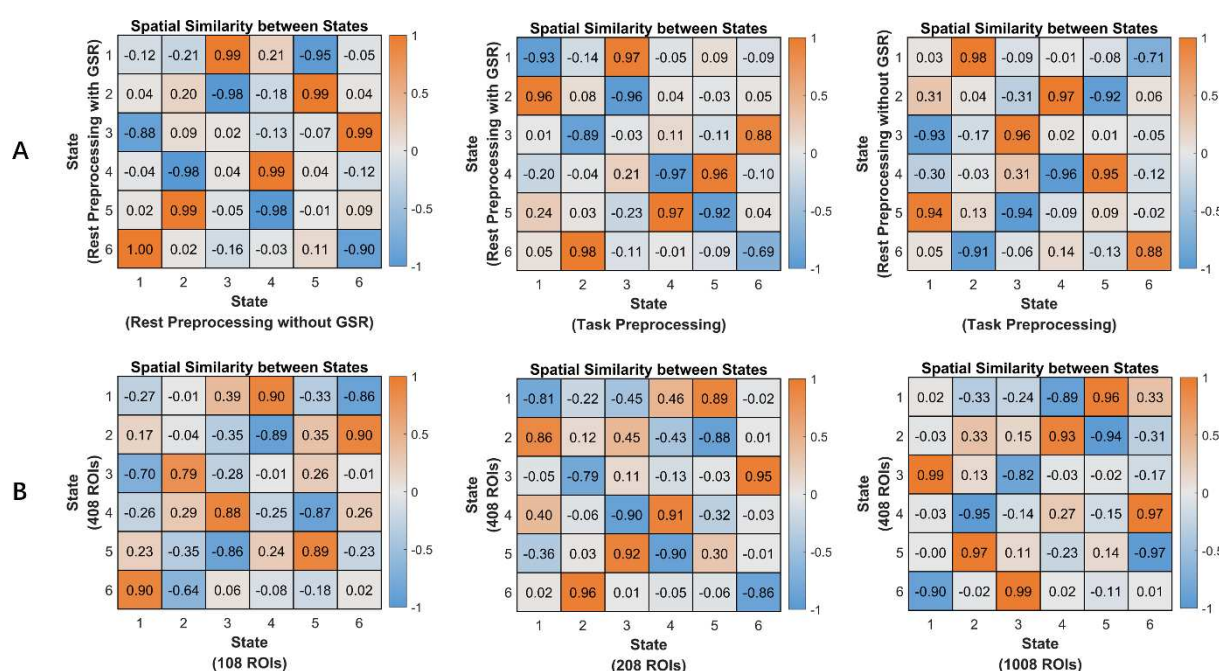
360

361

Figure 3. The CAP spatial similarity between states under A) different preprocessing

pipelines and B) different ROI numbers. The spatial similarity was measured by the Pearson

correction.

3.2.4. Temporal Reproducibility Evaluation

367   To verify the temporal reproducibility within the HC group more straightforwardly, all

368   states were relabeled to group corresponding states together. As shown in Figure 4, the

369   absolute values for the CAP metrics across different preprocessing pipelines, ROI numbers

14

370 and cohorts were evaluated in HC. As for the preprocessing pipeline, rest preprocessing with

371 and without GSR showed consistent results across all the three CAP metrics, while task

372 preprocessing showed shorter persistence and more counts. All three CAP metrics were not

373 sensitive to the ROI number. Different cohorts showed a consistent fraction of time and

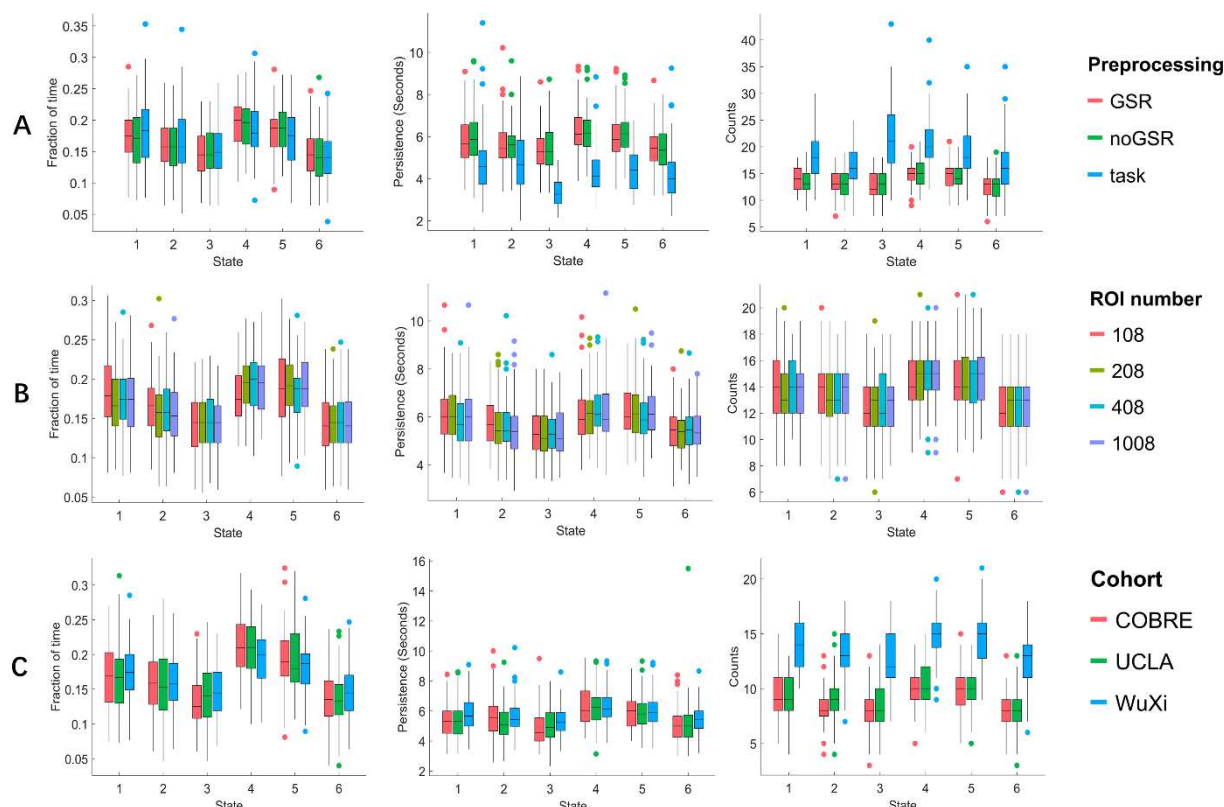374 persistence, and the WuXi cohort exhibited more counts than the other two cohorts.

375

377 **Figure 4.** The CAP metrics reproducibility within the HC group under different A)

378 preprocessing pipelines, B) ROI numbers and C) cohorts.

379

380 **3.3. Aberrant and Reproducible State Dynamics in Schizophrenia**

381 *3.3.1. State Temporal Dynamic Differences between SZ and HC*

382 The robust CAP analysis was applied to investigate the schizophrenia-related

383 abnormalities in the CAP dynamic state transition across three independent data cohorts. The

384 state temporal dynamics (CAP metrics) were compared between SZ patients and well-

385 matched HC controls by using a two-sample t-test, with age and gender as covariates. The

386 results of group comparisons were presented in Figure 5. As mentioned above, the six CAP

387 states could be grouped into three pairs (State 1 and 2, State 3 and 6, State 4 and 5). The mean

388 fraction of time of each state for SZ and HC groups was around 15% to 20%, and each state

389 persisted for 5 to 6 seconds. For example, the pair of State 4 and State 5 occupied the highest

15

390   fraction of time in both the SZ and HC groups, which shared opposite spatial coactivation

391   patterns dominated by SN, SMN and DMN. Almost every state except State 6 showed

392   significant temporal dynamic differences (P<0.05, FDR corrected). The group differences

393   were similar within each pair. For instance, SZ patients showed less fraction of time in states

394   characterized by FPN and DMN (State 1 and State 2), and more fraction of time in states

395   characterized by SN and DMN (State 4 and State 5).

396   Specifically, SZ patients showed a significantly reduced fraction of time and persistence

397   in State 1 and 2, as well as reduced counts in State 2, compared with the HC group (Figure

398   5A). In State 4 and 5, SZ patients had significantly increased fraction of time and counts.

399   Moreover, SZ patients showed a significantly increased fraction of time and counts in State 3,

400   but not in State 6. As for the transition probability between CAP states, SZ patients showed

401   lower transition probability from State 4 to State 2, and lower transition probability within

402   State 1 and State 2 (Figure 5B). On the other hand, SZ patients showed higher transition

403   probability from State 1 to State 5, State 2 to State 3, State 3 to State 5 and State 6 to State 4.

404   The detailed statistic values for these CAP metrics were described in Table S2, Supplementary
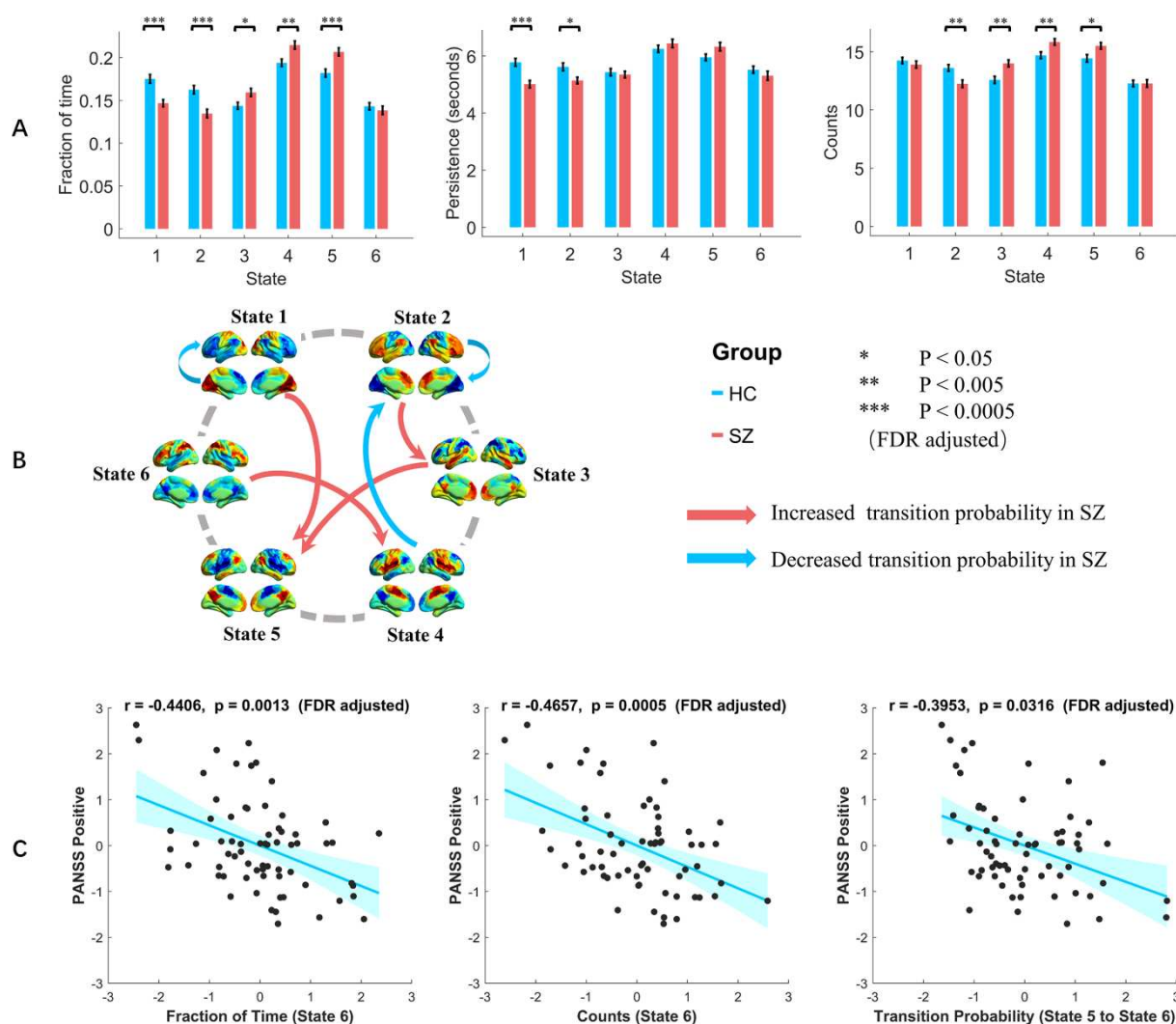
405   material.

406

16

Figure 5. State temporal dynamic differences between SZ and HC. The group differences in A) fraction of time, persistence, counts and B) transition probability. Red bins are the SZ group and blue bins are the HC group. Two-sample t-tests were performed with age and gender as covariates. Error-bar is the standard error. * indicates $p < 0.05$, and ** indicates $p < 0.005$, and *** indicates $p < 0.0005$ with FDR correction. For the transition probability, the red arrow means higher transition probability in the SZ group, and vice versa for the blue arrow. C) Behavioral relevance with state temporal dynamics in SZ. The fraction of time of State 6 was negatively correlated with the positive PANSS score, $r = -0.4406$, $p = 0.0013$; The counts of State 6 was negatively correlated with the positive PANSS score, $r = -0.4657$, $p = 0.0005$; The transition probability from State 5 to State 6 was negatively correlated with the positive PANSS score, $r = -0.3953$, $p = 0.0316$ (all the p values were FDR adjusted). The shadow represents the 95% confidence interval.

Abbreviations: PANSS, Positive and Negative Syndrome Scale.

3.3.2. The relationships between State Temporal Dynamics and Clinical Data

17

423   The clinical relevance with state temporal dynamics was evaluated in the SZ group,

424   using partial correlation with age and gender controlled. As shown in Figure 5C, after FDR

425   correction, the following negative correlations between CAP metrics and positive PANSS

426   score were found: the fraction of time of State 6 ($r = -0.4406$, $p = 0.0013$), the counts of State

427   6 ($r = -0.4657$, $p = 0.0005$), and the transition probability from State 5 to State 6 ($r = -0.3953$,

428      $p = 0.0316$). In addition, the persistence of State 3 ($r = -0.3388$, $p = 0.0323$) was negatively

429   correlated with the disease duration, the fraction of time of State 4 ($r = 0.3556$, $p = 0.0203$),

430   and the persistence of State 5 ($r = 0.3653$, $p = 0.0154$) was positively correlated with the

431   PANSS total score.

432

3.3.3. Reproducible Group Differences between SZ and HC

434   The reproducibility of SZ patients' dynamic alterations was also validated in this study,

435   which confirmed good temporal reproducibility for the group differences. For instance, SZ

436   showed more fraction of time in State 4 and State 5 and less fraction of time in State 1 and

437   State 2. These results were consistent across different methodological pipelines (Figure S5

438   and Figure S8, Supplementary material). And for the unchanged states under K = 6 (State 5)

439   and K = 8 (State 1), their temporal dynamic differences that SZ showed more fraction of time

440   than HC were consistent as well (Figure 6B).

441   Figure 7B showed the fraction of time differences between SZ and HC across the three

442   cohorts. Their overall trend among the six CAP states was similar, particularly State 2, State 3

443   and State 5 showed consistent significant group differences in the WuXi cohort and COBRE

444   cohort. Although the temporal dynamic differences obtained from the UCLA cohort were less

445   similar compared with the other two cohorts, the absolute values still showed a consistent

446   trend as presented in Figure 5C.

447   In addition, the repeatability for different cohorts was validated. Rather than using the

448   CAP maps from one cohort to the other cohorts, the CAP analysis was independently

449   performed for the COBRE and UCLA cohort, and the spatial and temporal results were

450   compared. Although the repeatability for different cohorts was relatively weaker, considerable

451   spatial overlaps were identified across the three cohorts. More details were described in

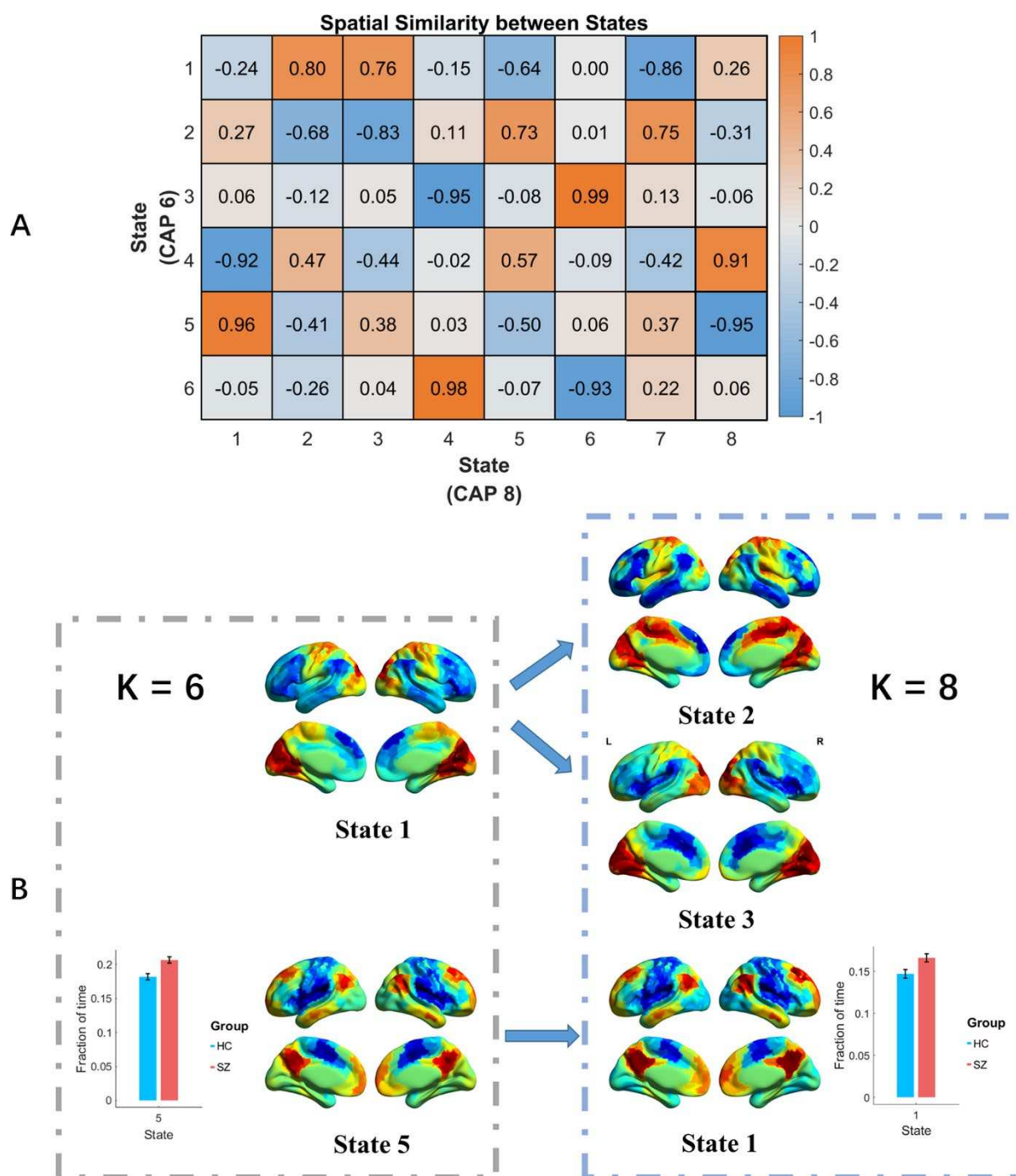452   Figure S11 to Figure S13, Supplementary material.

453

Figure 6. CAP analysis reproducibility with different cluster numbers. In this case, the configuration was WuXi cohort, rest preprocessing with GSR and 408 ROIs. A) The CAP spatial similarity between K = 6 and K = 8. B) The State 1 in K = 6 was divided into two states in K = 8, State 2 and State 3. State 5 in K = 6 remained in K = 8, which corresponds to State 1, and the SZ group also showed a consistent more fraction of time than the HC group. The error bar is the standard error.
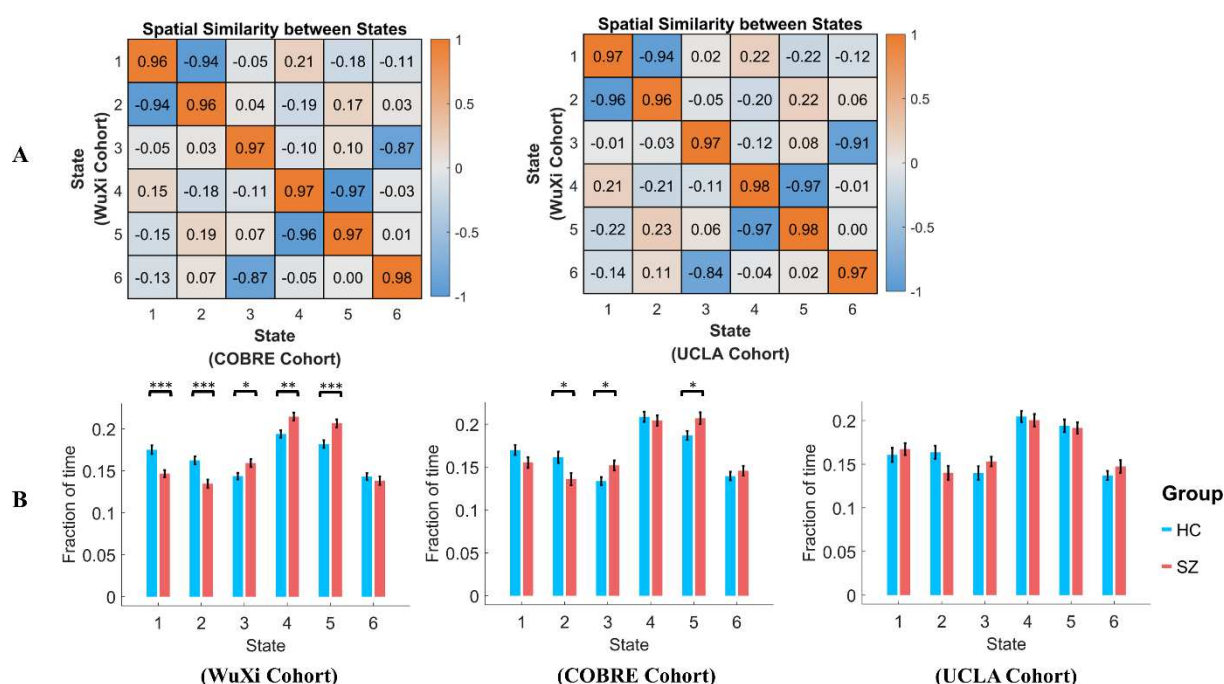
Figure 7. The generalizability of network dynamic measure differences between SZ and HC across the three independent cohorts. A) Applying the clustering results based on the WuXi cohort to the other two cohorts, their spatial similarity was measured by the Pearson correlation. B) The fraction of time differences between SZ and HC across the three cohorts. * indicates p < 0.05, ** indicates p < 0.005and *** indicates p < 0.005 (FDR adjusted). The error bar is the standard error.

4. Discussion

In this study, we first identified the characteristic and reliable states and transitions of functional brain networks in the healthy adults, and then investigated the schizophrenia-related aberrant state dynamics, based on the coactivation pattern analysis and three independent cohorts. Healthy and patient cohorts achieved robust results across different methodological pipelines. Our results revealed six reliable coactivation states of functional brain networks, which were constituted by typical resting-state networks including triple networks as well as primary and other higher-order networks. The principle of spontaneous state transitions inferred the higher spatial similarity, the higher transferring probability between the separable coactivation states. Patients with schizophrenia showed reproducible evidence of aberrant coactivation patterns dynamics, particularly the state dominance such as the fraction of time was altered and associated with positive symptoms in the patients. Together, our study confirms the reproducibility and generalizability of CAP analysis, which could provide meaningful information about the network dysfunction and neuropathological mechanisms in psychiatric disorders.

4.1. Coactivation Patterns for Brain States

The CAP analysis is based on the temporal k-means clustering of whole-brain functional activities, which identifies a group of spatial maps with similar whole-brain coactivation patterns across the whole scan. Motivated by the idea of PPA (Tagliazucchi et al., 2012), Liu et al. found that the DMN can be simply identified by averaging multiple distinct coactivations or co-deactivation patterns at different time points (Liu & Duyn, 2013). Yeo's 7 network parcellation was used in this study, and brain regions belonging to the same network tended to be activated or deactivated together (Figure 2). This result supports the intrinsic relationship between brain regions within the same functional network (B. B. Biswal et al., 2010; Calhoun & Adali, 2012), and these intrinsic networks can be simply extracted by averaging a few time points rather than using a more complex mathematical method such as ICA. Thus, while CAP states are derived from resting-state fMRI signals by using not pairwise functional connectivity but temporal clustering, which we feel at least partly represents the temporal dynamic characteristics of the whole-brain functional connectome (Zuo et al., 2012).

Previous ICA analyses used to divide the DMN network into anterior part and posterior part (B. B. Biswal et al., 2010; Zuo et al., 2010). Our results also found the posterior DMN (mainly includes the precuneus/posterior cingulate cortex and angular gyrus) and the anterior DMN (mainly includes the medial prefrontal cortex) were activated at different level across states. The posterior DMN tends to be related to the SN and SMN (State 4 and 5), while the anterior DMN was associated with FPN and DAN (State 3 and 6). Besides, three pairs of states were identified with opposite coactivation patterns. For instance, when DMN was activated, the FPN and DAN were deactivated (State 3), and vice versa is true for State 6. The phenomenon of opposite CAP pairs has also been found in previous studies (Huang et al., 2020; Janes et al., 2020; Zhang et al., 2020), suggesting these regions tend to be activated in an opposite manner that the activation of region A would suppress the activity of another region B, and vice versa.

The DMN is known as the task-negative network. For State 3 to State 6, when DMN was activated, other task-positive networks such as FPN and SN were either not activated or deactivated. These results verified the anti-correlation between the task-positive network and the task-negative network (Fox et al., 2005; Power et al., 2011). Based on CAPs, Li and colleagues concatenated a set of task activation maps from the Human Connectome Project, and validated the robust anti-correlated functional network (DMN) across multiple tasks (Li et

519   al., 2020). However, we found that the DMN was not always activated conversely compared

520   with FPN. Specifically, the medial-prefrontal subsystem and temporal subsystem of DMN

521   were co-deactivated with FPN when the visual network was activated, and vice versa is true

522   (State 1 and State 2). This is consistent with recent findings that the DMN and FPN are

523   coactivated when evaluating internal information (Beaty et al., 2016; Zhu et al., 2017) and

524   involved in task preparation (Koshino et al., 2011).

525

526   **4.2. Transition Probability and Spatial Similarity**

527   Unlike the Pearson correlation matrix which is mathematically symmetric, the transition

528   probability between State A and State B is not equal. Nevertheless, a significant positive

529   correlation was obtained ($r = 0.8479$, $p < 0.0001$) between the transition probability pairs,

530   suggesting the transition probability between two states is an approximation (Figure 4A). In

531   addition, the transition probability between two states was significantly correlated with their

532   spatial similarity ($r = 0.9817$, $p < 0.0001$), which suggests that one state would transfer to the

533   other state with a higher probability. This positive association was also found by a previous

534   study based on the hidden Markov model (Vidaurre et al., 2017), as the brain should activate

535   continuously, it is less likely that one CAP state would directly change to another state with

536   opposite whole-brain coactivation configuration without any intermediate state.

537

538   **4.3. Reproducibility in CAPs Analysis and Results**

539   In this study, we considered the reproducibility of our analyses from several aspects,

540   including preprocessing pipeline, ROI number, cluster number and cohort, and they showed

541   consistent results.

542   For CAP analysis based on resting-state fMRI data, currently there is no standard

543   preprocessing pipeline. Some studies used the common task preprocessing pipeline, which

544   mainly includes realignment, spatial normalization and smoothing (Kaiser et al., 2019;

545   Karahanoglu & Van De Ville, 2015). More studies used the standard resting-state

546   preprocessing pipeline, which has additional steps such as nuisance signal regression (WM,

547   CSF) and temporal filtering, with and without GSR (Karahanoglu & Van De Ville, 2015; Liu

548   et al., 2013; Liu & Duyn, 2013; Ma et al., 2020). We used both the task and resting-state

549   preprocessing pipelines (with and without GSR) in this study. As shown in Figure 3 and

550   Figure 4, similar coactivation patterns and temporal dynamics were obtained for different

551   preprocessing pipelines, which suggests the preprocessing has little effect on the whole-brain

552   coactivation patterns. Besides, as Figure 4A showed, task preprocessing has shorter

553   persistence and more counts. The reason could be that the high-frequency noise (Chen &

554   Glover, 2015) was not filtered during the task preprocessing, which causes frequent

555   fluctuations and shorter persistence.

556   Both voxel-level (Liu et al., 2013) and ROI-level (Janes et al., 2020) were studied in

557   previous CAP analysis studies. Using ROI could reduce the dimension and save a lot of time

558   and computational resources (Chen et al., 2015), while it could also decrease the spatial

559   resolution and ignore spatial details. We chose different ROI numbers from 100, 200, 400 to

560   1000 to represent multiple levels of ROI size. As shown in Figure 3 and Figure 4, the

561   coactivation patterns showed highly spatial and temporal dynamics consistency, suggesting

562   that the CAP analysis is not sensitive to the spatial resolution.

563   As for the cluster number, when increasing the cluster number, the spatial and temporal

564   properties change continuously. For instance, when K increased from 6 to 8, four states

565   remained the overall spatial coactivation patterns, and their temporal dynamics were also

566   unchanged (Figure 6).

567   Besides the analytic variations, we also validated the results obtained from the three

568   independent cohorts. Although the spatial consistency of coactivation patterns between

569   cohorts was less than that of different preprocessing steps, there were still considerable spatial

570   overlaps. To further verify the generalizability of our findings, we mapped the CAP maps

571   obtained by the WuXi cohort to the other two cohorts, and the group temporal dynamic

572   differences between SZ and HC were similar across cohorts (Figure 7B). In conclusion, our

573   study suggested there was considerable reproducibility across different analytic variations and

574   cohorts.

575

576   **4.4. State Temporal Dynamics Abnormalities in Schizophrenia and Their**

577   **Reproducibility**

578   Using the robust CAP spatial maps, the state temporal dynamics in terms of fraction of

579   time, persistence, counts, and transition probability were calculated and compared between

580   SZ and HC groups. Reproducible and aberrant state temporal dynamic was found in

581   schizphrenia patients concerning different methodological pipelines or cohorts (Figure 5 - 7).

582   Most CAP states demonstrated aberrant dynamic characteristics, suggesting schizophrenia-

583   related network dysfunction is widespread over the whole brain, which is consistent with the

584   accumulating evidence that schizophrenia is characterized by whole-brain network

585   dysfunction (Adhikari et al., 2019; Collin et al., 2016; Fornito et al., 2012; Kambeitz et al.,

586   2016; Venkataraman et al., 2012). Previous fMRI studies reported that schizophrenia patients

587 showed distributed alterations in the dynamic functional connectivity (Du et al., 2018),

588 dynamic brain activity (Fu et al., 2018) and dynamic state (Allen et al., 2014; Damaraju et al.,

589 2014; Fu et al., 2020; Mennigen et al., 2018; Rashid et al., 2014). A recent resting-state fMRI

590 study revealed dysregulated brain dynamics, i.e., reduced, less persistent, and more variable

591 between-network interactions among SN, FPN and DMN in schizophrenia (Supekar et al.,

592 2019), which proves aberrant triple network saliency model of psychosis (V. J. W. P. Menon,

593 2020). Our findings extend the current understanding about schizophrenia-related dynamic

594 abnormalities in such manner that aberrant state temporal dynamics in schizophrenia is

595 associated with not only triple networks but also part of primary (VN, SMN) and higher-order

596 networks (DAN).

597   First, we found that SZ patients had insufficiently intensified activation and less inhibited

598 deactivation in FPN-DMN state, but on the contrary for SN-DMN state, of which the

599 transition probability changed significantly. It has been well documented that, the triple

600 networks, involving FPN, SN and DMN, are the cores for higher cognition. Specifically, FPN

601 is engaged in externally oriented attention during demanding cognitive tasks, SN is crucial in

602 the process of salience mapping, and DMN is related to self-referential processes (V. Menon,

603 2011). Imaging findings based on triple network alterations have enhanced our understanding

604 of the psychopathology in schizophrenia, depression and autism (Krishnadas et al., 2014;

605 Manoliu et al., 2014; Nekovarova et al., 2014; Supekar et al., 2019; J. Wang et al., 2020).

606 Recent meta-analysis confirms that the triple network might underlie the common network

607 dysfunction across psychiatric disorders including schizophrenia (Sha et al., 2019). Although

608 our findings highlight schizophrenia-related dynamic abnormalities centered in the triple

609 network, in line with an earlier study (Supekar et al., 2019), our results further point out that

610 the DMN was continuously activated across all states while SN and FPN were only involved

611 with specific states, which may suggest the DMN play a crucial role in the state transitions

612 and cross-network interactions within the triple networks.

613   Second, we found that the robust CAP states were also centered in the primary networks

614 such as VN and SMN, and higher-order network such as DAN, which had substantially

615 altered temporal state dynamics in schizophrenia patients. Interestingly, the VN, SMN, and

616 DAN were recently identified across psychiatric disorders, by partial least squares which is a

617 different data-driven approach from CAP analysis, as key parts underlying the general

618 psychopathology, cognitive dysfunction, and impulsivity (Kebets et al., 2019). In this study,

619 Kebets and colleagues found the latent components of whole-brain resting-state functional

620 connectivity were robust, and particularly, SMN showed featured alterations in the static

24

resting-state functional connectivity within and between networks. Our study provides consistent evidence for schizophrenia-related network dysfunction from a new perspective of CAP states and state transition. Furthermore, we reported that the dynamic characteristics of the FPN-DAN state (State 6) were negatively correlated with the PANSS positive scores, and those of SN-DMN state (State 4 and 5) were positively correlated with the PANSS total scores, consistent with previous evidence (Kindler et al., 2015; Manoliu et al., 2013; Pang et al., 2017; Rotarska-Jagiela et al., 2010; D. H. Wang et al., 2018). Importantly, the transition probability from the SN-DMN state (State 5) to the FPN-DAN state (State 6) was also negatively correlated with the positive PANSS scores. Notably, the group difference was not significant for State 6 (Figure 5A). This finding may suggest that the state transition is likely to alleviate the disease severity from the symptom positively-related state to the symptom negatively-related state, which might provide a potential intervention target for schizophrenia patients. Taken together, the reproducible abnormalities of state temporal dynamics identified in this study implicate that schizophrenia is associated with whole-brain functional network dysregulation and dynamic alterations.

4.5. Limitations

Although the k-means clustering has been widely used in fMRI data, currently there is no optimal criterion to determine the cluster number (Vergara et al., 2020). In this study, the volume numbers for the WuXi, COBRE and UCLA cohort are 240, 150 and 152 respectively, with the same TR. When we increased the cluster number in the CAP analysis, the average volumes allocated to each cluster (state) decreased, which might cause more variability for each cluster and reduce the clustering stability. In the COBRE and UCLA cohort, we tested the k-means clustering from 2 to 21, and for K = 21 there are only average 7 volumes for a single state, which had too limited temporal information. Therefore, we chose the K = 6 following the qualitative but arbitrary criteria in line with the prior study (Liu & Duyn, 2013).

5. Conclusion

In summary, functional brain states involved with specific coactivation patterns at different time points were obtained using coactivation pattern analysis. The spatial and temporal reproducibility of these CAPs was verified from multiple aspects, such as different preprocessing pipelines and independent cohorts. Moreover, the robust and aberrant temporal dynamics were identified in schizophrenia, associated with the severity of clinical symptoms. This study proved that the CAP analysis has good reproducibility and generalizability, which

655   is useful to provide novel and robust information about aberrant brain dynamic configurations

656   for understanding the psychopathological mechanisms in schizophrenia.

657

658   **Ethics Statement**

659   All participants provided informed written consent. This research was approved by the

660   respective Universities/Hospitals depending on the origin of the dataset (Medical Ethics

661   Committee of Wuxi Mental Health Center, Nanjing Medical University for the WuXi cohort,

662   Institutional Review Boards at UCLA and the Los Angeles County for the UCLA cohort, and

663   institutional review board protocols of the University of New Mexico for the COBRE cohort).

664   This study was conducted in accordance with the Declaration of Helsinki guidelines.

665

666   **Conflict of Interest**

667   The authors declare no conflict of interest.

668

669   **Data and Code Availability Statements**

670   The two open cohorts were obtained from UCLA Consortium for Neuropsychiatric

671   Phenomics LA5c Study (https://openneuro.org/datasets/ds000030/versions/1.0.0) and The

672   Center for Biomedical Research Excellence (COBRE)

673   (http://fcon_1000.projects.nitrc.org/indi/retro/cobre.html). The WuXi cohort is not publicly

674   available due to privacy or ethical restrictions. The code that supports the findings of this

675   study will be made available upon request from the corresponding author.

676

677   **Acknowledgements**

684

References

Adhikari, B. M., Hong, L. E., Sampath, H., Chiappelli, J., Jahanshad, N., Thompson, P. M., et al. (2019). Functional network connectivity impairments and core cognitive deficits in schizophrenia. *Hum Brain Mapp, 40*(16), 4593-4605. doi:10.1002/hbm.24723

Allen, E. A., Damaraju, E., Plis, S. M., Erhardt, E. B., Eichele, T., & Calhoun, V. D. (2014). Tracking Whole-Brain Connectivity Dynamics in the Resting State. *Cerebral Cortex, 24*(3), 663-676. doi:10.1093/cercor/bhs352

Aurich, N. K., Alves Filho, J. O., Marques da Silva, A. M., & Franco, A. R. (2015). Evaluating the reliability of different preprocessing steps to estimate graph theoretical measures in resting state fMRI data. *Front Neurosci, 9*, 48. doi:10.3389/fnins.2015.00048

Beaty, R. E., Benedek, M., Silvia, P. J., & Schacter, D. L. (2016). Creative Cognition and Brain Network Dynamics. *Trends Cogn Sci, 20*(2), 87-95. doi:10.1016/j.tics.2015.10.004

Biswal, B., Yetkin, F. Z., Haughton, V. M., & Hyde, J. S. (1995). Functional Connectivity in the Motor Cortex of Resting Human Brain Using Echo-Planar Mri. *Magnetic Resonance in Medicine, 34*(4), 537-541. doi:DOI 10.1002/mrm.1910340409

Biswal, B. B., Mennes, M., Zuo, X. N., Gohel, S., Kelly, C., Smith, S. M., et al. (2010). Toward discovery science of human brain function. *Proc Natl Acad Sci U S A, 107*(10), 4734-4739. doi:10.1073/pnas.0911855107

Botvinik-Nezer, R., Holzmeister, F., Camerer, C. F., Dreber, A., Huber, J., Johannesson, M., et al. (2020). Variability in the analysis of a single neuroimaging dataset by many teams. *Nature, 582*(7810), 84-88. doi:10.1038/s41586-020-2314-9

Bowring, A., Maumet, C., & Nichols, T. E. (2019). Exploring the impact of analysis software on task fMRI results. *Hum Brain Mapp, 40*(11), 3362-3384. doi:10.1002/hbm.24603

Calhoun, V. D., & Adali, T. (2012). Multisubject independent component analysis of fMRI: a decade of intrinsic networks, default mode, and neurodiagnostic discovery. *IEEE Rev Biomed Eng, 5*, 60-73. doi:10.1109/RBME.2012.2211076

Chen, J. E., Chang, C., Greicius, M. D., & Glover, G. H. (2015). Introducing co-activation pattern metrics to quantify spontaneous brain network dynamics. *Neuroimage, 111*, 476-488. doi:10.1016/j.neuroimage.2015.01.057

Chen, J. E., & Glover, G. H. (2015). BOLD fractional contribution to resting-state functional connectivity above 0.1 Hz. *Neuroimage, 107*, 207-218. doi:10.1016/j.neuroimage.2014.12.012

Collin, G., Turk, E., & van den Heuvel, M. P. (2016). Connectomics in Schizophrenia: From Early Pioneers to Recent Brain Network Findings. *Biol Psychiatry Cogn Neurosci Neuroimaging, 1*(3), 199-208. doi:10.1016/j.bpsc.2016.01.002

Damaraju, E., Allen, E. A., Belger, A., Ford, J. M., McEwen, S., Mathalon, D. H., et al. (2014). Dynamic functional connectivity analysis reveals transient states of dysconnectivity in schizophrenia. *Neuroimage Clin, 5*, 298-308. doi:10.1016/j.nicl.2014.07.003

Di, X., & Biswal, B. B. (2015). Characterizations of resting-state modulatory interactions in the human brain. *J Neurophysiol, 114*(5), 2785-2796. doi:10.1152/jn.00893.2014

Du, Y., Fryer, S. L., Fu, Z., Lin, D., Sui, J., Chen, J., et al. (2018). Dynamic functional connectivity impairments in early schizophrenia and clinical high-risk for psychosis. *Neuroimage, 180*(Pt B), 632-645. doi:10.1016/j.neuroimage.2017.10.022

Eklund, A., Nichols, T. E., & Knutsson, H. (2016). Cluster failure: Why fMRI inferences for spatial extent have inflated false-positive rates. *Proceedings of the National Academy of Sciences of the United States of America, 113*(28), 7900-7905. doi:10.1073/pnas.1602413113

735 Esteban, O., Markiewicz, C. J., Blair, R. W., Moodie, C. A., Isik, A. I., Erramuzpe, A., et al.
736   (2019). fMRIPrep: a robust preprocessing pipeline for functional MRI. *Nat Methods,*
737   *16*(1), 111-116. doi:10.1038/s41592-018-0235-4
738 Fong, A. H. C., Yoo, K., Rosenberg, M. D., Zhang, S., Li, C. S. R., Scheinost, D., et al.
739   (2019). Dynamic functional connectivity during task performance and rest predicts
740   individual differences in attention across studies. *Neuroimage, 188*, 14-25.
741   doi:10.1016/j.neuroimage.2018.11.057
742 Fornito, A., Zalesky, A., Pantelis, C., & Bullmore, E. T. (2012). Schizophrenia, neuroimaging
743   and connectomics. *Neuroimage, 62*(4), 2296-2314.
744   doi:10.1016/j.neuroimage.2011.12.090
745 Fox, M. D., Snyder, A. Z., Vincent, J. L., Corbetta, M., Van Essen, D. C., & Raichle, M. E.
746   (2005). The human brain is intrinsically organized into dynamic, anticorrelated
747   functional networks. *Proceedings of the National Academy of Sciences of the United*
748   *States of America, 102*(27), 9673-9678. doi:10.1073/pnas.0504136102
749 Freitas, L. G. A., Bolton, T. A. W., Krikler, B. E., Jochaut, D., Giraud, A. L., Huppi, P. S., et
750   al. (2020). Time-resolved effective connectivity in task fMRI: Psychophysiological
751   interactions of Co-Activation patterns. *Neuroimage, 212*, 116635.
752   doi:10.1016/j.neuroimage.2020.116635
753 Friston, K. J. (2011). Functional and effective connectivity: a review. *Brain Connect, 1*(1), 13-
754   36. doi:10.1089/brain.2011.0008
755 Fu, Z., Iraji, A., Turner, J. A., Sui, J., Miller, R., Pearlson, G. D., et al. (2020). Dynamic state
756   with covarying brain activity-connectivity: On the pathophysiology of schizophrenia.
757   *Neuroimage, 224*, 117385. doi:10.1016/j.neuroimage.2020.117385
758 Fu, Z., Tu, Y., Di, X., Du, Y., Pearlson, G. D., Turner, J. A., et al. (2018). Characterizing
759   dynamic amplitude of low-frequency fluctuation and its relationship with dynamic
760   functional connectivity: An application to schizophrenia. *Neuroimage, 180*(Pt B), 619-
761   631. doi:10.1016/j.neuroimage.2017.09.035
762 Gonzalez-Castillo, J., & Bandettini, P. A. (2018). Task-based dynamic functional connectivity:
763   Recent findings and open questions. *Neuroimage, 180*(Pt B), 526-533.
764   doi:10.1016/j.neuroimage.2017.08.006
765 Huang, Z., Zhang, J., Wu, J., Mashour, G. A., & Hudetz, A. G. (2020). Temporal circuit of
766   macroscale dynamic brain activity supports human consciousness. *Sci Adv, 6*(11),
767   eaaz0087. doi:10.1126/sciadv.aaz0087
768 Hunt, M. J., Kopell, N. J., Traub, R. D., & Whittington, M. A. (2017). Aberrant Network
769   Activity in Schizophrenia. *Trends Neurosci, 40*(6), 371-382.
770   doi:10.1016/j.tins.2017.04.003
771 Hutchison, R. M., Womelsdorf, T., Allen, E. A., Bandettini, P. A., Calhoun, V. D., Corbetta,
772   M., et al. (2013). Dynamic functional connectivity: Promise, issues, and
773   interpretations. *Neuroimage, 80*, 360-378. doi:10.1016/j.neuroimage.2013.05.079
774 Janes, A. C., Peechatka, A. L., Frederick, B. B., & Kaiser, R. H. (2020). Dynamic functioning
775   of transient resting-state coactivation networks in the Human Connectome Project.
776   *Hum Brain Mapp, 41*(2), 373-387. doi:10.1002/hbm.24808
777 Kaiser, R. H., Kang, M. S., Lew, Y., Van Der Feen, J., Aguirre, B., Clegg, R., et al. (2019).
778   Abnormal frontoinsular-default network dynamics in adolescent depression and
779   rumination: a preliminary resting-state co-activation pattern analysis.
780   *Neuropsychopharmacology, 44*(9), 1604-1612. doi:10.1038/s41386-019-0399-3
781 Kambeitz, J., Kambeitz-Ilankovic, L., Cabral, C., Dwyer, D. B., Calhoun, V. D., van den
782   Heuvel, M. P., et al. (2016). Aberrant Functional Whole-Brain Network Architecture in
783   Patients With Schizophrenia: A Meta-analysis. *Schizophr Bull, 42 Suppl 1*, S13-21.
784   doi:10.1093/schbul/sbv174

Karahanoglu, F. I., & Van De Ville, D. (2015). Transient brain activity disentangles fMRI resting-state dynamics in terms of spatially and temporally overlapping networks. *Nature Communications, 6*, 7751. doi:10.1038/ncomms8751

Kebets, V., Holmes, A. J., Orban, C., Tang, S., Li, J., Sun, N., et al. (2019). Somatosensory-Motor Dysconnectivity Spans Multiple Transdiagnostic Dimensions of Psychopathology. *Biol Psychiatry, 86*(10), 779-791. doi:10.1016/j.biopsych.2019.06.013

Kindler, J., Jann, K., Homan, P., Hauf, M., Walther, S., Strik, W., et al. (2015). Static and Dynamic Characteristics of Cerebral Blood Flow During the Resting State in Schizophrenia. *Schizophrenia Bulletin, 41*(1), 163-170. doi:10.1093/schbul/sbt180

Koshino, H., Minamoto, T., Ikeda, T., Osaka, M., Otsuka, Y., & Osaka, N. (2011). Anterior medial prefrontal cortex exhibits activation during task preparation but deactivation during task execution. *Plos One, 6*(8), e22909. doi:10.1371/journal.pone.0022909

Krishnadas, R., Ryali, S., Chen, T., Uddin, L., Supekar, K., Palaniyappan, L., et al. (2014). Resting state functional hyperconnectivity within a triple network model in paranoid schizophrenia. *Lancet, 383*, 65-65.

Li, M., Dahmani, L., Wang, D., Ren, J., Stocklein, S., Lin, Y., et al. (2020). Co-activation patterns across multiple tasks reveal robust anti-correlated functional networks. *Neuroimage, 227*, 117680. doi:10.1016/j.neuroimage.2020.117680

Liu, X., Chang, C., & Duyn, J. H. (2013). Decomposition of spontaneous brain activity into distinct fMRI co-activation patterns. *Front Syst Neurosci, 7*, 101. doi:10.3389/fnsys.2013.00101

Liu, X., & Duyn, J. H. (2013). Time-varying functional network information extracted from brief instances of spontaneous brain activity. *Proc Natl Acad Sci U S A, 110*(11), 4392-4397. doi:10.1073/pnas.1216856110

Ma, X., Zhuo, Z., Wei, L., Ma, Z., Li, Z., Li, H., et al. (2020). Altered Temporal Organization of Brief Spontaneous Brain Activities in Patients with Alzheimer's Disease. *Neuroscience, 425*, 1-11. doi:10.1016/j.neuroscience.2019.11.025

Manoliu, A., Riedl, V., Doll, A., Bauml, J. G., Muhlau, M., Schwerthoffer, D., et al. (2013). Insular Dysfunction Reflects Altered Between-Network Connectivity and Severity of Negative Symptoms in Schizophrenia during Psychotic Remission. *Front Hum Neurosci, 7*, 216. doi:10.3389/fnhum.2013.00216

Manoliu, A., Riedl, V., Zherdin, A., Muhlau, M., Schwerthoffer, D., Scherr, M., et al. (2014). Aberrant dependence of default mode/central executive network interactions on anterior insular salience network activity in schizophrenia. *Schizophr Bull, 40*(2), 428-437. doi:10.1093/schbul/sbt037

Mennigen, E., Miller, R. L., Rashid, B., Fryer, S. L., Loewy, R. L., Stuart, B. K., et al. (2018). Reduced higher-dimensional resting state fMRI dynamism in clinical high-risk individuals for schizophrenia identified by meta-state analysis. *Schizophrenia Research, 201*, 217-223. doi:10.1016/j.schres.2018.06.007

Menon, V. (2011). Large-scale brain networks and psychopathology: a unifying triple network model. *Trends Cogn Sci, 15*(10), 483-506. doi:10.1016/j.tics.2011.08.003

Menon, V. J. W. P. (2020). Brain networks and cognitive impairment in psychiatric disorders. *19*(3), 309.

Nekovarova, T., Fajnerova, I., Horacek, J., & Spaniel, F. (2014). Bridging disparate symptoms of schizophrenia: a triple network dysfunction theory. *Front Behav Neurosci, 8*, 171. doi:10.3389/fnbeh.2014.00171

Pang, L. J., Kennedy, D., Wei, Q. L., Lv, L. X., Gao, J. S., Li, H., et al. (2017). Decreased Functional Connectivity of Insular Cortex in Drug Naive First Episode Schizophrenia: In Relation to Symptom Severity. *Plos One, 12*(1). doi:ARTN e0167242
10.1371/journal.pone.0167242

Power, J. D., Cohen, A. L., Nelson, S. M., Wig, G. S., Barnes, K. A., Church, J. A., et al. (2011). Functional Network Organization of the Human Brain. *Neuron, 72*(4), 665-678. doi:10.1016/j.neuron.2011.09.006

Preti, M. G., Bolton, T. A. W., & Van De Ville, D. (2017). The dynamic functional connectome: State-of-the-art and perspectives. *Neuroimage, 160*, 41-54. doi:10.1016/j.neuroimage.2016.12.061

Rashid, B., Damaraju, E., Pearlson, G. D., & Calhoun, V. D. (2014). Dynamic connectivity states estimated from resting fMRI Identify differences among Schizophrenia, bipolar disorder, and healthy control subjects. *Frontiers in Human Neuroscience, 8*. doi:ARTN 897

10.3389/fnhum.2014.00897

Rotarska-Jagiela, A., van de Ven, V., Oertel-Knochel, V., Uhlhaas, P. J., Vogeley, K., & Linden, D. E. J. (2010). Resting-state functional network correlates of psychotic symptoms in schizophrenia. *Schizophrenia Research, 117*(1), 21-30. doi:10.1016/j.schres.2010.01.001

Rousseeuw, P. J. (1987). Silhouettes: a graphical aid to the interpretation and validation of cluster analysis. *Journal of Computational and Applied Mathematics, 20*(1), 53-65.

Schaefer, A., Kong, R., Gordon, E. M., Laumann, T. O., Zuo, X. N., Holmes, A. J., et al. (2018). Local-Global Parcellation of the Human Cerebral Cortex from Intrinsic Functional Connectivity MRI. *Cereb Cortex, 28*(9), 3095-3114. doi:10.1093/cercor/bhx179

Sha, Z., Wager, T. D., Mechelli, A., & He, Y. (2019). Common Dysfunction of Large-Scale Neurocognitive Networks Across Psychiatric Disorders. *Biol Psychiatry, 85*(5), 379-388. doi:10.1016/j.biopsych.2018.11.011

Shirer, W. R., Jiang, H., Price, C. M., Ng, B., & Greicius, M. D. (2015). Optimization of rs-fMRI Pre-processing for Enhanced Signal-Noise Separation, Test-Retest Reliability, and Group Discrimination. *Neuroimage, 117*, 67-79. doi:10.1016/j.neuroimage.2015.05.015

Smith, S. M., Miller, K. L., Moeller, S., Xu, J., Auerbach, E. J., Woolrich, M. W., et al. (2012). Temporally-independent functional modes of spontaneous brain activity. *Proc Natl Acad Sci U S A, 109*(8), 3131-3136. doi:10.1073/pnas.1121329109

Strother, S. C. (2006). Evaluating fMRI preprocessing pipelines - Review of preprocessing steps for BOLD fMRI. *Ieee Engineering in Medicine and Biology Magazine, 25*(2), 27-41. doi:Doi 10.1109/Memb.2006.1607667

Supekar, K., Cai, W., Krishnadas, R., Palaniyappan, L., & Menon, V. (2019). Dysregulated Brain Dynamics in a Triple-Network Saliency Model of Schizophrenia and Its Relation to Psychosis. *Biol Psychiatry, 85*(1), 60-69. doi:10.1016/j.biopsych.2018.07.020

Tagliazucchi, E., Balenzuela, P., Fraiman, D., & Chialvo, D. R. (2012). Criticality in large-scale brain FMRI dynamics unveiled by a novel point process analysis. *Front Physiol, 3*, 15. doi:10.3389/fphys.2012.00015

Tian, L., Meng, C., Jiang, Y., Tang, Q., Wang, S., Xie, X., et al. (2016). Abnormal functional connectivity of brain network hubs associated with symptom severity in treatment-naive patients with obsessive–compulsive disorder: A resting-state functional MRI study. *66*, 104-111.

Tzourio-Mazoyer, N., Landeau, B., Papathanassiou, D., Crivello, F., Etard, O., Delcroix, N., et al. (2002). Automated anatomical labeling of activations in SPM using a macroscopic anatomical parcellation of the MNI MRI single-subject brain. *Neuroimage, 15*(1), 273-289. doi:10.1006/nimg.2001.0978

Venkataraman, A., Whitford, T. J., Westin, C. F., Golland, P., & Kubicki, M. (2012). Whole brain resting state functional connectivity abnormalities in schizophrenia. *Schizophrenia Research, 139*(1-3), 7-12. doi:10.1016/j.schres.2012.04.021

Vergara, V. M., Mayer, A. R., Damaraju, E., Hutchison, K., & Calhoun, V. D. (2017). The effect of preprocessing pipelines in subject classification and detection of abnormal resting state functional network connectivity using group ICA. *Neuroimage, 145*, 365-376. doi:10.1016/j.neuroimage.2016.03.038

Vergara, V. M., Salman, M., Abrol, A., Espinoza, F. A., & Calhoun, V. D. (2020). Determining the number of states in dynamic functional connectivity using cluster validity indexes. *Journal of Neuroscience Methods, 337*. doi:ARTN 108651

10.1016/j.jneumeth.2020.108651

Vidaurre, D., Quinn, A. J., Baker, A. P., Dupret, D., Tejero-Cantero, A., & Woolrich, M. W. (2016). Spectrally resolved fast transient brain states in electrophysiological data. *Neuroimage, 126*, 81-95. doi:10.1016/j.neuroimage.2015.11.047

Vidaurre, D., Smith, S. M., & Woolrich, M. W. (2017). Brain network dynamics are hierarchically organized in time. *Proc Natl Acad Sci U S A, 114*(48), 12827-12832. doi:10.1073/pnas.1705120114

Wang, D. H., Li, M. L., Wang, M. Y., Schoeppe, F., Ren, J. X., Chen, H. F., et al. (2018). Individual-specific functional connectivity markers track dimensional and categorical features of psychotic illness (vol 25, 2119, 2020). *Molecular Psychiatry, 25*(9), 2200-2200. doi:10.1038/s41380-018-0340-x

Wang, J., Wang, Y., Huang, H., Jia, Y., Zheng, S., Zhong, S., et al. (2020). Abnormal dynamic functional network connectivity in unmedicated bipolar and major depressive disorders based on the triple-network model. *Psychol Med, 50*(3), 465-474. doi:10.1017/S003329171900028X

Yeo, B. T., Krienen, F. M., Sepulcre, J., Sabuncu, M. R., Lashkari, D., Hollinshead, M., et al. (2011). The organization of the human cerebral cortex estimated by intrinsic functional connectivity. *J Neurophysiol, 106*(3), 1125-1165. doi:10.1152/jn.00338.2011

Zalesky, A., Fornito, A., Cocchi, L., Gollo, L. L., & Breakspear, M. (2014). Time-resolved resting-state brain networks. *Proc Natl Acad Sci U S A, 111*(28), 10341-10346. doi:10.1073/pnas.1400181111

Zhang, J., Huang, Z., Tumati, S., & Northoff, G. (2020). Rest-task modulation of fMRI-derived global signal topography is mediated by transient coactivation patterns. *PLoS Biol, 18*(7), e3000733. doi:10.1371/journal.pbio.3000733

Zhu, W., Chen, Q., Xia, L., Beaty, R. E., Yang, W., Tian, F., et al. (2017). Common and distinct brain networks underlying verbal and visual creativity. *Hum Brain Mapp, 38*(4), 2094-2111. doi:10.1002/hbm.23507

Zuo, X. N., Biswal, B. B., & Poldrack, R. A. (2019). Editorial: Reliability and Reproducibility in Functional Connectomics. *Front Neurosci, 13*, 117. doi:10.3389/fnins.2019.00117

Zuo, X. N., Ehmke, R., Mennes, M., Imperati, D., Castellanos, F. X., Sporns, O., et al. (2012). Network centrality in the human functional connectome. *Cereb Cortex, 22*(8), 1862-1875. doi:10.1093/cercor/bhr269

Zuo, X. N., Kelly, C., Adelstein, J. S., Klein, D. F., Castellanos, F. X., & Milham, M. P. (2010). Reliable intrinsic connectivity networks: Test-retest evaluation using ICA and dual regression approach. *Neuroimage, 49*(3), 2163-2177. doi:10.1016/j.neuroimage.2009.10.080